LA-UR-23-29999

Approved for public release; distribution is unlimited.

Title:	A Progress Report for a 44-month Aging Study on Nitroplasticizer (NP) Stability - Summary of DFT and FTIR Results
Author(s):	Yang, Dali Jung, Julie Cathy Antoinette Odile Gonzales, Ivana O'Neel, Jillian Cathleen Torres, Joseph Angelo
Intended for:	Report
Issued:	2023-09-01

A Progress Report for a 44-month Aging Study on Nitroplasticizer (NP) Stability – Summary of DFT and FTIR Results

Dali Yang[a], Julie Jung[b], Ivana Matanovic[b], Jillian C. O'Neel[a], and Joseph A. Torres[a]

[a]MST-7: Engineered Materials, Material Sciences and Technology Division
[b]T-1: Physics and Chemistry of Materials, Theoretical Division
Los Alamos National Laboratory, Los Alamos, NM 87545, USA

Abstract: In the past few years, a 44-month long aging experiment was conducted under various aging conditions. The properties of aged nitroplasticizer (NP) samples were analyzed using Fourier transform infrared spectroscopy, Karl Fischer (KF) titration, thermogravimetric analysis (TGA), liquid chromatography tandem quadrupole time of flight mass spectrometry (LC/QTOF), and ion chromatography (IC). In this progress report, some FTIR results are documented and discussed. On the theoretical front, density functional theory (DFT) calculations were carried out. Some DFT results are discussed as well.

1. Introduction

In the formulation of 9501 PBX, a binder that consists of 2.5 wt% nitroplasticizer and 2.5 wt% Estane, is commonly used to bind the energetic crystals together for propellant and explosive fabrications. Nitroplasticizer studied here is the eutectic mixture of bis-2,2-dinitropropyl acetal (BDNPA) and bis-2,2-dinitropropyl formal (BDNPF), with a weight ratio of approximately 1:1 (hereinafter called NP) [1, 2]. The molecular structures of BDNPA and BDNPF are given in Figure 1. NP also contains a trace amount of N-phenyl-β-naphthylamine (PBNA) (~0.1 wt%) for the purpose of long-term storage, which was added after NP production for scavenging NO_x radicals and oxidants generated from NP degradation [3]. The molecular structure of PBNA is also given in Figure 1. Like many plasticizers with a low molecular weight, NP has a tendency to diffuse out of the PBX matrix and decompose at moderate temperatures after prolonged aging into reactive by-products, such as NO, NO_2, H_2O, HONO, HNO_3, N_2O, and other NP residuals. Through oxidation and hydrolysis, the reactive molecules can further degrade NP, NP residues, and nearby polymeric materials, which cause undesired impacts. Understanding how NP degradation initiates and progresses is a critical prerequisite for understanding how to control the aging condition and to prevent NP and hence polymers from degradation during storage, handling, manufacturing, and application stages. Toward this goal, we conducted the present 44-month aging experiment with improved experimental design. Over the aging process, the properties of aged samples are characterized by using coulometric Karl Fischer (KF) titration and Near Infrared (NIR), thermogravimetric analysis (TGA), Fourier transform infrared spectroscopy (FTIR). In the 1st progress report, we documented and discussed the TGA and KF results [4]. In this progress report, the results of FTIR analyses for the same set of aged NP samples are documented and discussed. To add more insights on different degradation mechanisms which might occur during NP aging, density functional theory (DFT) calculations were performed. Some of these results will be discussed.

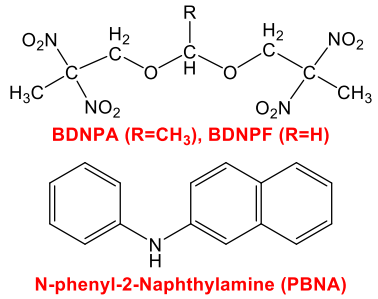

Figure 1. Molecular structures of BDNPA, BDNPF, and PBNA.

2. Experiment

2.1. Aging sample preparation

Baseline NP was obtained from a newly opened drum (lot number OCP–A/F–XB 8/8), which was made around 1965 and stored at LANL. At the beginning of this aging experiment, this baseline NP has been naturally aged for more than 51 years. As expect, some degradation has taken place during the storage, such as the depletion of PBNA (as low as ~760 mM) and increased water concentration (~780 ppm (wt/wt)). After the production, the pristine NP contains 0.1 wt% PBNA (= 6.33 mM) and <600 ppm water [5]. The baseline NP was used to prepare all aged samples, which had been aged in dry air and under nitrogen (N_2) conditions (called dry samples), and in direct contact with deionized (DI) water (called wet samples). Each set of samples was loaded into two different types of containers: one type - IR cells (32 SIR1, Firefly Sci.com) for NIR measurements in a pseudo-in-situ mode; and second type - glass vials (12x32 clean vials with screw caps, Fisher) for TGA/KF/MIR/LC-QTOF/IC measurements. The samples aged inside the cells were capped with a Teflon stopper secured with two layers of Teflon tape. Evidentially, this seal was imperfect so that some volatiles were able to leak out of the cells, hence they are referred to as leaked samples. For the vial samples, Teflon tape was added between the thread and the cap to ensure the tightness of the seal, hence they were referred to as sealed samples. All cell and vial samples were kept inside Teflon containers. Four sets of samples were respectively heated at 38, 45, 55, and 64°C up to 44 months. The full suite of analyses was performed at twenty points during the aging experiment. More details on the preparation procedure of the aging samples, description, and visual observation can be found elsewhere [6, 7]. For clarification of discussion, Table 1 summarizes the labelling method of all samples, aging environments, and characterization techniques applied to the samples.

Table 1. Summary of sample labelling, aged environments, and characterization techniques*.

	Container	Environment	Short label	Characterization
Sealed sample	Glass vial	Air and N_2	Dry	TGA, KF, MIR, LC/QFOT, IC
		DI water	Wet	TGA, KF, MIR, LC/QFOT, IC
Leaked sample	IR cell	Air and N_2	Dry	NIR
		DI water	Wet	NIR

*: At 44 months, after the NIR measurement, the aged samples were removed from the NIR cells for MIR and LC/QTOF analyses, but TGA and KF analyses were not conducted due to limited sample size (<0.28 ml of liquid sample in each cell).

A Thermo Nicolet™ iS50 FTIR spectrometer was used to perform MIR in an attenuated total reflectance (ATR) mode with a diamond crystal between 4000 and 450 cm^{-1}. The resolution of 4 cm^{-1} and 16 scans were used. The Thermo OMNIC™ software was used to process the MIR results. For each sample, two to four spectra were collected, and the average spectrum was used for data analysis.

3. Computational methods

All electronic structure calculations were performed using DFT, with the BP86 functional and the DEF2-TZVPP basis set as implemented in the *ab initio* quantum chemistry program ORCA 5.0.3 [8, 9]. The description of dispersion interactions was included through Grimme's atom-pairwise dispersion correction [10] and Becke-Johnson damping (D3BJ). All BDNPA/F structures were optimized with tight settings, i.e., tight convergence criteria for the electronic energy calculations and geometry optimizations. The transition states were located with the quadratic synchronous transit technique using the structures for the reactant and product. For each structure, a frequency calculation is performed to confirm that the resulting geometry corresponds to a minimum (positive frequencies) or a first order saddle point (one mode with imaginary frequency) on the potential energy surface. For NO_2 homolysis the transition state is identified as a triplet electronic state. The solvation effect in NP was introduced using conductor-like polarizable continuum model [11] with refractive index set to 1.45 [12] and dielectric constant set to 15.4 [13]. Optimized geometries are used to compute the thermodynamic properties and evaluate Helmholtz free energy for primary elementary step to start the degradation of BDNPA/F via three degradation reactions: HONO elimination, NO_2 homolysis, and BFNPF/A hydrolysis. We focus on the Helmholtz free energies, rather than the Gibbs free energies, because the experiments are run at constant volume and not constant pressure. For each structure, the Helmholtz free energy (F) is computed at various temperatures in the range of 25-60 °C. The reaction Helmholtz free energies are obtained as the difference in Helmholtz free energy between the products and the reactants, for example $\boldsymbol{\Delta}F = F(\mathrm{C}) + F(\mathrm{D}) - F(\mathrm{A}) - F(\mathrm{B})$ for the reaction $\mathrm{A} + \mathrm{B} \rightarrow \mathrm{C} + \mathrm{D}$. The kinetic barriers were calculated as the Helmholtz free energy difference between the reaction transition state and the reactant. It is worth noting that the performance of the PB86 functional was evaluated by comparing with kinetic barriers to the ones calculated using MP2 level of theory with a DEF2-TZVPP basis set, which should provide a valid estimate for the range of values that could be obtained with different choice of functionals. The comparison shows that the MP2 calculated kinetic barriers are consistently larger (for ~30%) than the ones calculated with DFT, indicating that the relative values (differences in calculated numbers for different systems or reactions) will not be strongly dependent on the choice of the functional. This is in agreement with previous work [14, 15] that reported errors for BP86 barrier height calculations between 35 kJ/mol and 84 kJ/mol.

4. Results and Discussion

4.1. DFT Calculation Results

Because BDNPA/F have four NO_2 groups, HONO elimination can lead to four different products: (trans, right), (cis, right), (trans, left) and (cis, right), as shown on the right-hand side of Figure 2 in which the results obtained from BDNPA are presented. The calculated Helmholtz free energies for four cases are

negative, which means the HONO elimination is an exothermic reaction though trans configurations (left or right) are more energetically favorable than cis configurations. Since the trans-products give the lowest Helmholtz free energy (<-12 kJ/mol), as shown on the left-hand side of Figure 2. The trans-products will be used in the following DFT calculation and discussion.

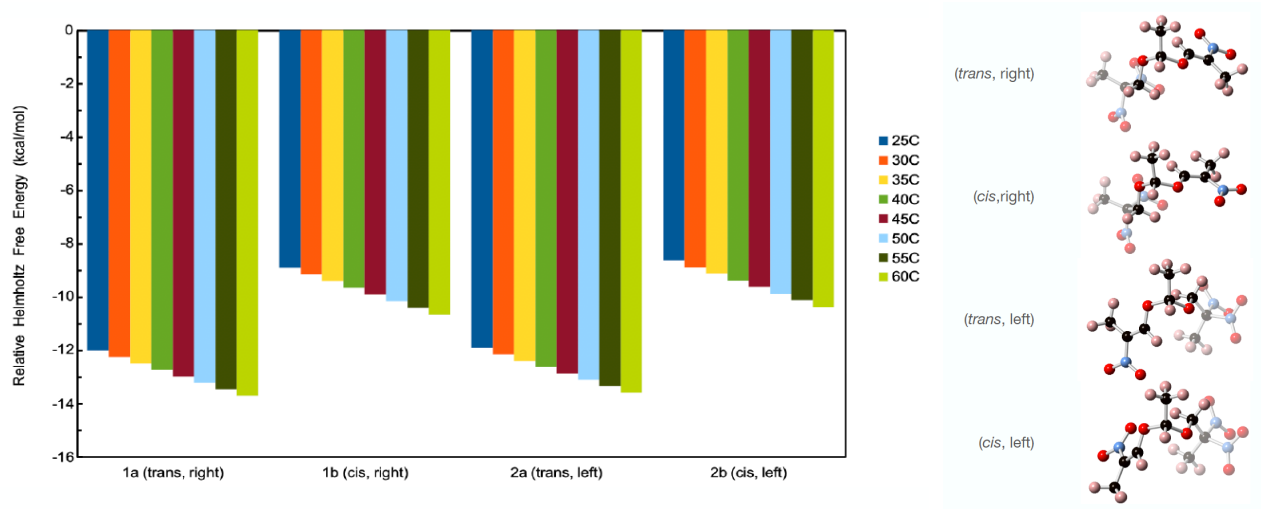

Figure 2**.** The calculated Helmholtz free energies for four configurations. The 3D molecular structures of these four configurations are illustrated on the right-hand side.

Table 2 summarizes the DFT calculated change in Helmholtz free energy for HONO elimination and NO_2 homolysis together with the kinetic barriers calculated for the two reactions. The results further show that HONO elimination is an exothermic process and will release -50.3 and -56.2 kJ/mol in energy, in the case of BDNPA and BDNPF, respectively. The energy barrier, also called activation energy, for the HONO elimination reaction in BDNPA and BDNPF are similar, 114.2 and 109.6 kJ/mol, respectively. These results explain why the BDNPA/F ratio is often observed unchanged in the early stage when both actually undergo HONO elimination. Therefore, the BDNPA/F ratio should not be used as an indicator to monitor the degree of NP degradation.

Table 2. Summary of DFT calculated activation energy and Helmholtz free energy associated with the HONO elimination and the NO2 homolysis reaction in NP degradation.

Reaction	**HONO Elimination**		**NO_2 Homolysis**	
Chemical	BDNPA	BDNPF	BDNPA	BDNPF
Activation energy (kJ/mol)	114.2	109.6	230.3	231.3
Free energy (*ΔF*) (kJ/mol)	-50.3	-56.2	93.4	88.3
	Exothermic		**Endothermic**	

The DFT calculation also shows that NO_2 homolysis is an endothermic process, which requires 93.4 and 88.3 kJ/mol of energy in the case of the BDNPA and BDNPF molecule, respectively. DFT calculations also show that NO_2 homolysis requires more than double the energy barrier than HONO elimination. Namely, the kinetic barrier for NO_2 homolysis is calculated as 230.3 kJ/mol for BDNPA

and 231.3 kJ/mol for BDNPF, respectively. The results show that the BDNPA/F degradation *via* the NO_2 homolysis is much less likely to happen than the HONO elimination. Coincidentally, the DFT calculations also suggest that the Helmholtz free energy change for HONO elimination and NO_2 homolysis in BDNPF is slightly smaller than in BDNPA. Furthermore, it is worth emphasizing that HONO elimination and NO_2 homolysis can happen on either end of the molecule and the present full molecule model corroborates a previous assumption that the kinetic barrier on one end of the molecule is independent of the other end [16], which allows us to write the HONO elimination reaction as NP → NP' + 2HONO. Hence, the DFT results reveal the Helmholtz Free Energy for the elimination of two HONO is almost equivalent to twice the Helmholtz Free Energy for the elimination of only one HONO from a half molecule model of BDNPA, which indicates that one end of the molecule does not influence the other end.

The DFT calculated change in Helmholtz free energy for HONO elimination together with the kinetic barriers and concluded that HONO elimination is more energetically favorable over other degradation mechanisms, like NO_2 homolysis. Furthermore, it is suggested that HONO could react back to form two possible isomers, nitroso alcohol (HO-R-R_o-NO) and nitrite (R-ONO), when the HONO formed in close proximity to the decomposed fragments due to the cage effect (e.g., minimal headspace) [16, 17]. We calculated Helmholtz free energy for HONO re-addition to BDNPA molecules. As the previous work suggested, HONO can be re-added as HO-NO or H-ONO (i.e., HO-C1-C2-NO or H-C1-C2-ONO). For each configuration, there is four possible conformations (front-front (a), front-back (b) back-front (c), and back-back (d)), as shown in Figure 3. In total, there are for the sixteen of possible BDNPA isomers. Considering the lowest energy state of the trans form, the HONO re-addition is only tested for the left-trans configuration of BDNPA(-HONO). Considering overall isomerization reaction of BDNPA through HONO elimination and subsequent re-addition, the calculated Helmholtz free energies are plotted in Figure 4 for the 16 possible BDNPA isomers. The temperature effect is evaluated from 25°C to 60°C. Among these isomers formed via HO-NO re-addition is more energetically favorable than H-ONO re-addition, which agrees with the previous results [16, 18, 19]. Among the isomers via HO-ON re-addition, the configurations denoted NO-OH_2a and NO-OH_2d give the lowest Helmholtz free energies.

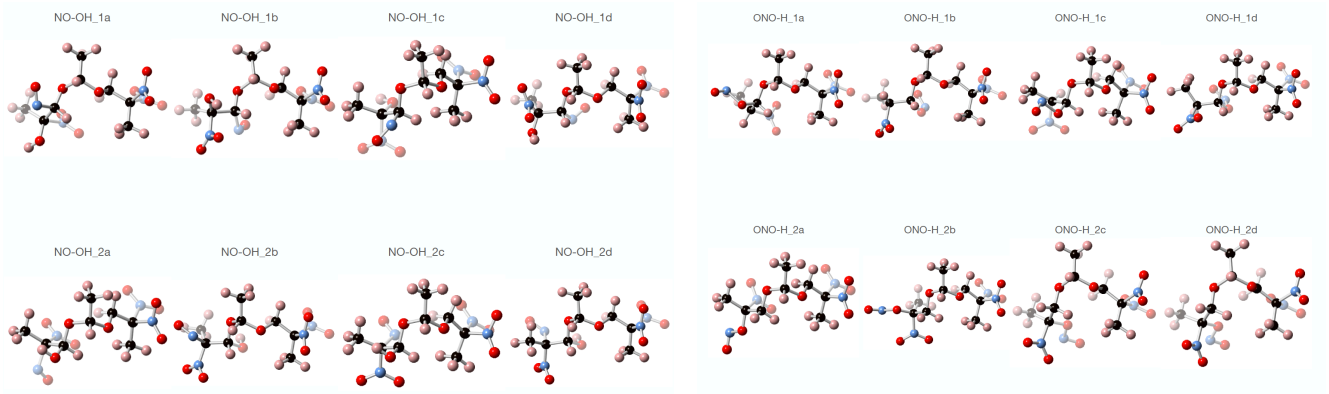

Figure 3**.** Isomers formed by HONO re-addition via HO-NO addition (left) and H-ONO addition (right) into the left-trans BDNPA-HONO configuration. For each configuration, there are four possible conformations (front-front (a), front-back (b) back-front (c), and back-back (d)).

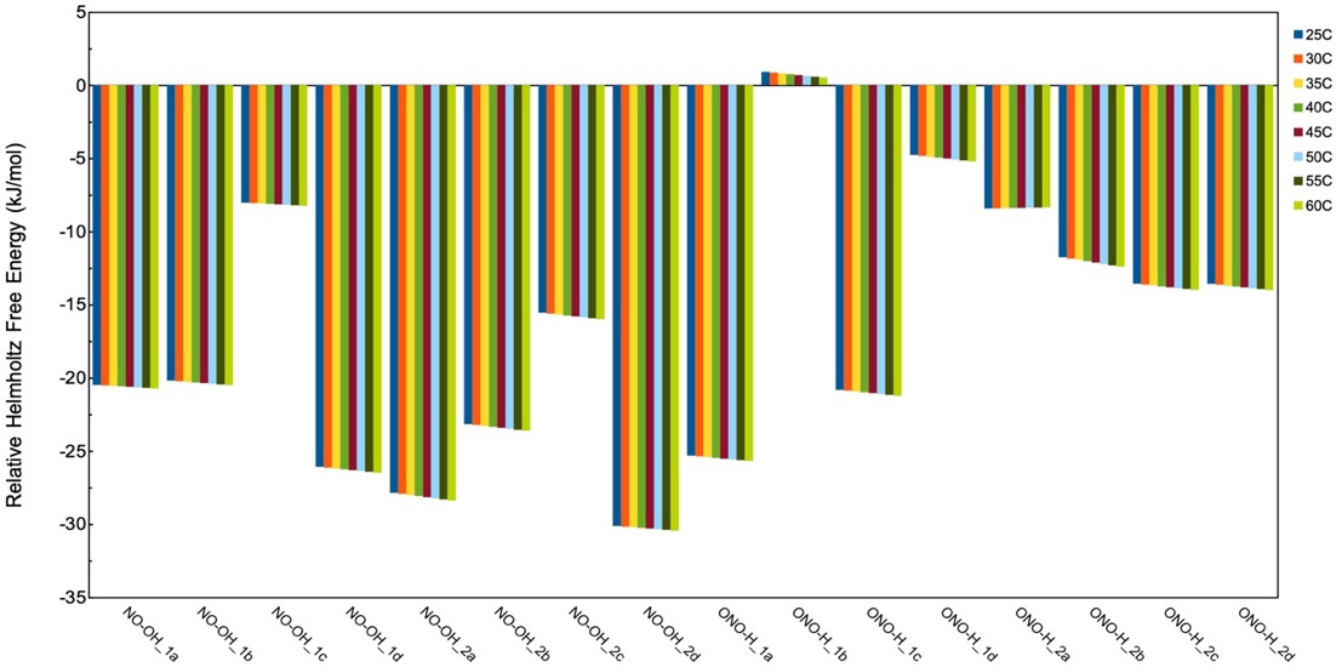

Figure 4. Helmholtz free energies of overall isomerization reaction of BDNPA through HONO elimination and subsequent re-addition into the left-trans BDNPA-HONO configuration. The temperature effect is evaluated.

Next, we investigated the protonation reaction of BDNPA/F with hydronium (Figure 5a) and water molecules (Figure 5b) as reactants, which will start the hydrolysis degradation reaction. As the local conditions and thus the effective dielectric function, of NP could change during the aging process, we plotted the Helmholtz free energy for the protonation of BDNPA as a function of dielectric constant of the system. We also explored how Helmholtz free energy for the protonation reaction changes with the change in the proton concentration, i.e., ratio of proton and water molecules ($[H_3O^+]/[H_2O]$). The results show that the protonation of BDNPA, and therefore the hydrolysis reaction, is strongly dependent on the local acidity conditions. On the contrary, without a proton, water molecules will not protonate BDNPA as the energy required for this process is larger than 250 kJ/mol. Evidently, the presence of protons is crucial to start hydrolysis degradation reaction. For example, for the dielectric constant set to 15.4 and in excess of water molecules ($[H_3O^+]/[H_2O]$ ratio of 10^{-6}), the change in the Helmholtz free energy for the protonation of BDNPA is calculated as 33.7 kJ/mol. However, the Helmholtz free energy for the BDNPA protonation decreases as the concentration of H_3O^+ increases and becomes exothermic when the $[H_3O^+]/[H_2O]$ ratio falls below 0.8. The dielectric constant also influences the energetics of the protonation reaction. Namely, a low value of dielectric constant (more nonpolar environment) benefits the protonation rection and the Helmholtz free energy for the BDNPA protonation at $[H_3O^+]/[H_2O] = 10^{-6}$ decreases from 33.7 to 4.2 kJ/mol as the dielectric constant decreases from 15.4 to 2.5. The Helmholtz free energy for the protonation of BDNPA and BDNPF (Figure 5c) shows larger differences in free energy as compared to the HONO elimination and NO_2 homolysis reaction. Helmholtz free energy for the protonation of BDNPF is calculated as 51.1 and 17.3 kJ/mol for $[H_3O^+]/[H_2O]$ ratios of 10^{-6} and 1, respectively, as compared to the value of 33.7 and -0.5 kJ/mol calculated for BDNPA. Unlike the

degradation of BDNPA through HONO elimination, this result shows that the degradation of BDNPA via hydrolysis is expected to be more pronounced than the degradation of BDNPF and will accelerate at high proton concentrations (high acidity).

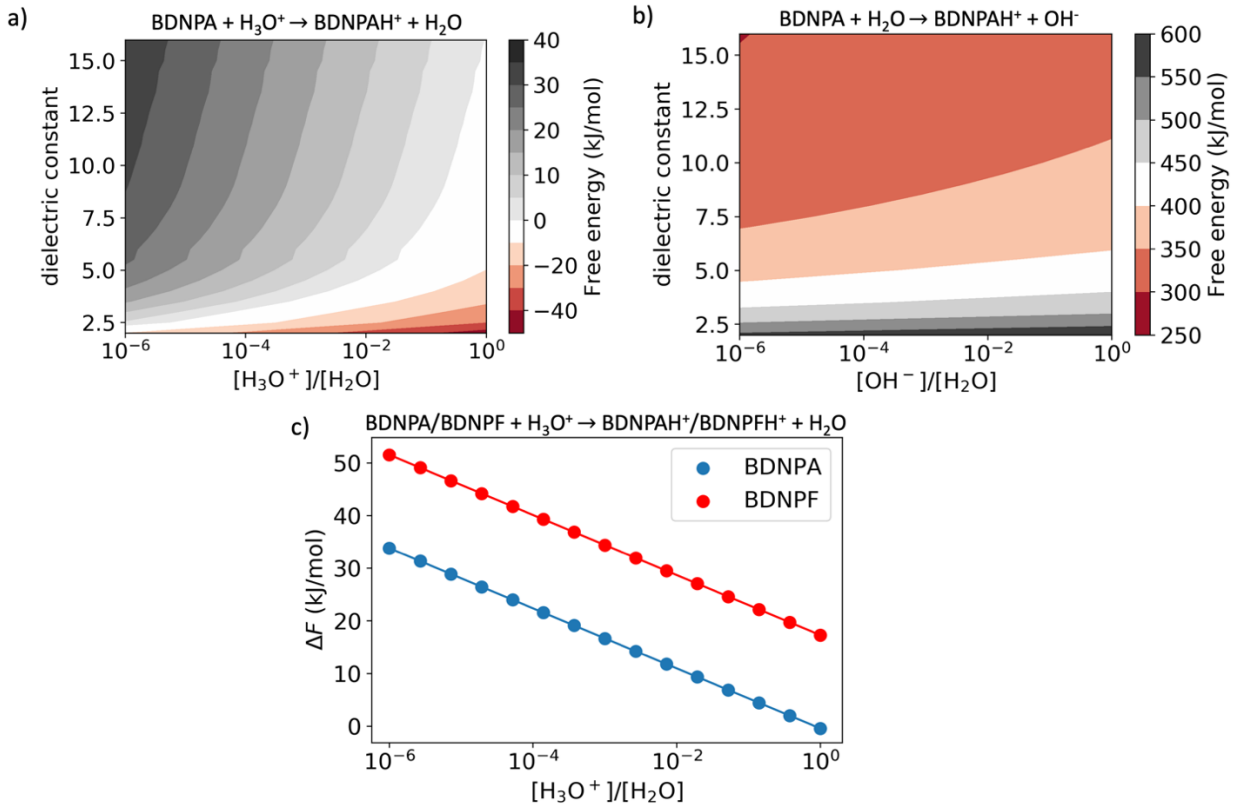

Figure 5. Helmholtz free energy for a) protonation of BDNPA from H_3O^+ as a function of dielectric constant and H_3O^+/H_2O concentration, b) protonation of BDNPA from H_2O as a function of dielectric constant and OH^-/H_2O concentration, and c) dependence of the Helmholtz free energy for BDNPA and BDNPF protonation on the ratio of protons and water for $\varepsilon = 15.4$. Calculated using BP86-D3BJ/DEF2-TZVPP level of theory.

4.2. FTIR Results

4.2.1 Temperature effect

Figure 6 shows the FTIR spectra of the baseline NP and the dry samples aged inside the glass vials for 44 months at 38 °C (3A), 45 °C (4A), 55 °C (5A), and 64 °C (6A). For better illustration, the FTIR spectra are divided into two regions: high wavenumber (HWN: 4000–2350 cm^{-1}) and low wavenumber (LWN: 1850–450 cm^{-1}). The tentative assignments of important peaks in BDNPA, BDNPF, and degraded fragments are summarized in Tables 2(a) and 2(b). Since the baseline NP has been aging for more than 51 years during its storage, it already contains acidic molecules (HONO and oxalic acids) [20] and an extra amount of water [6, 7]. A recent Pantex's report evidenced that NP gains its acidity and water concentration during the storage, compared to the pristine NP [21, 22]. In the FTIR spectrum of the baseline NP, while HONO might be responsible for the weak peak at ~3600 cm^{-1} [23], the weak peaks at 3678 and 3260 cm^{-1} are for large water clusters and small water clusters, respectively [24]. The

formation of the water cluster in NP was previously reported by Salazar et. al. and the cluster of 5 water molecules was used in their water sorption study in NP [25]. Additionally, the baseline spectrum shows a broad shoulder between 3200 and 3400 cm^{-1}, which indicates the presence of -OH groups, due to the formation of free vs. hydrogen bonded (H-bonded) water, and water clusters [24, 26], and also influenced by impurities and degraded PBNA products [21, 27]. After aging at 38°C and 45°C for 44 months, the changes in the FTIR spectra of the aged samples are minimal compared to that of the baseline NP. Some intensity increase in the region of 2550 cm^{-1} is most likely associated with the formation of HNO_X from a small degree of NP degradation.

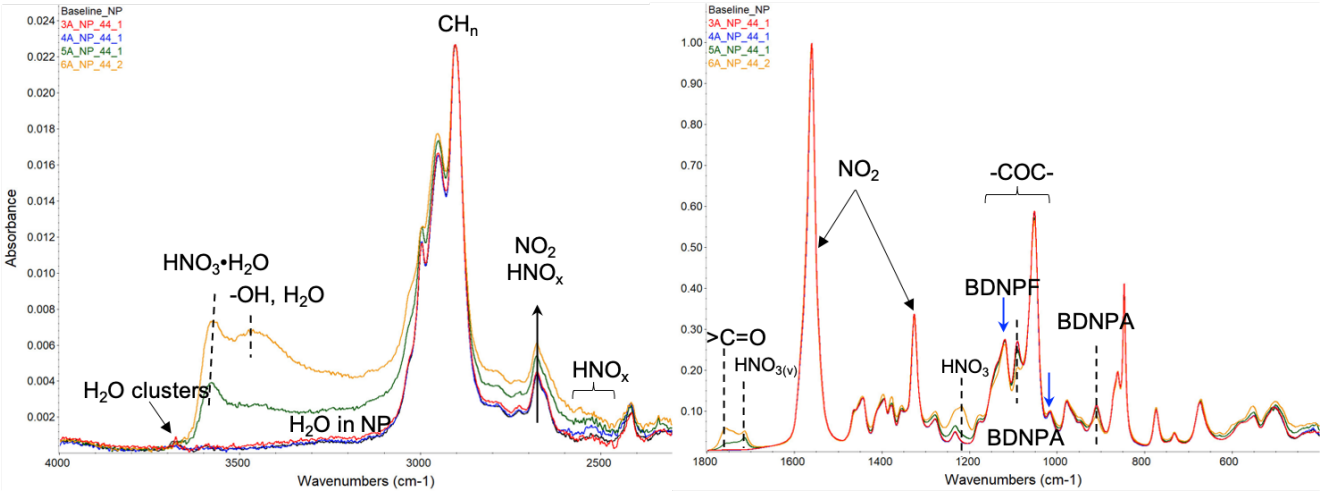

Figure 6. FTIR of the dry (air) samples aged for 44 months at different temperatures. All spectra are normalized at highest peak respective to the HWN and LWN regions.

More obvious changes are observed in the FTIR spectra of samples aged at 55°C and 64°C for 44 months. New peaks and shoulders grow between 3700 cm^{-1} and 3200 cm^{-1}, suggesting the formation of HNO_3 (at ~3580 cm^{-1}) and the presence of different forms of water molecules (free vs. H-bonded) [24, 26, 28], alcohols (e.g., DNPOH), and organic acids [20]. New peaks form between 1800 cm^{-1} and 1700 cm^{-1}, suggesting the formation of aliphatic ester (>C=O, at ~1760 cm^{-1}) and carboxylic acid (~1730 cm^{-1}) [29], and $HNO_{3(vapor)}$ (~1710 cm^{-1}) [28]. Changes in the intensity of numerous peaks between 1600 cm^{-1} and 450 cm^{-1} suggest changes in the backbone structure of NP due to oxidation and hydrolysis [18, 19, 30]. More specifically, while the peaks at 1710 cm^{-1} and 1340 cm^{-1}, associated with HNO_3 molecules, grow noticeably, the peak at 1092 cm^{-1}, associated with the -COC(CH_3)- group in BDNPA, decreases greatly. This observation suggests that as more HNO_3 forms, BDNPA degrades severely, supporting the acid-catalyzed hydrolysis hypothesis. Relatively speaking, the intensity of the peaks at 1050 and 1120 cm^{-1}, associated with the -COC- group in BDNPF, does not change significantly. Similar behaviors and features are found in the FTIR spectra of the N_2 and wet samples, as shown in Figure 7 and Figure 8. All these results confirm that 1) temperature plays an important role in degrading NP regardless of the environmental conditions, and 2) 55°C seems to be a transition point for the different aging behavior occurring in NP because the wet sample ages less than the dry samples at 55°C and below. However, at 64°C, whereas the wet sample does hydrolyze more than the dry samples (air and N_2), the dry samples

are oxidized more (the higher >C=O peak intensity at ~1760 cm^{-1}) than the wet sample. All these FTIR results agree with the KF and TGA results [4], the NIR results [6, 7], and the IC results [20].

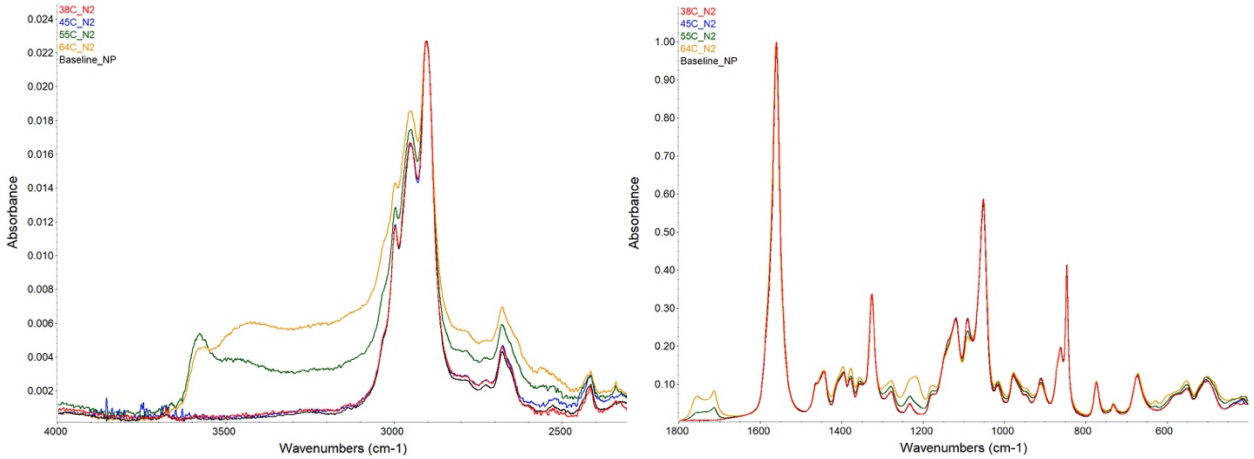

Figure 7. FTIR of the dry (N_2) samples aged for 44 months at different temperatures. All spectra are normalized at highest peak respective to the HWN and LWN regions.

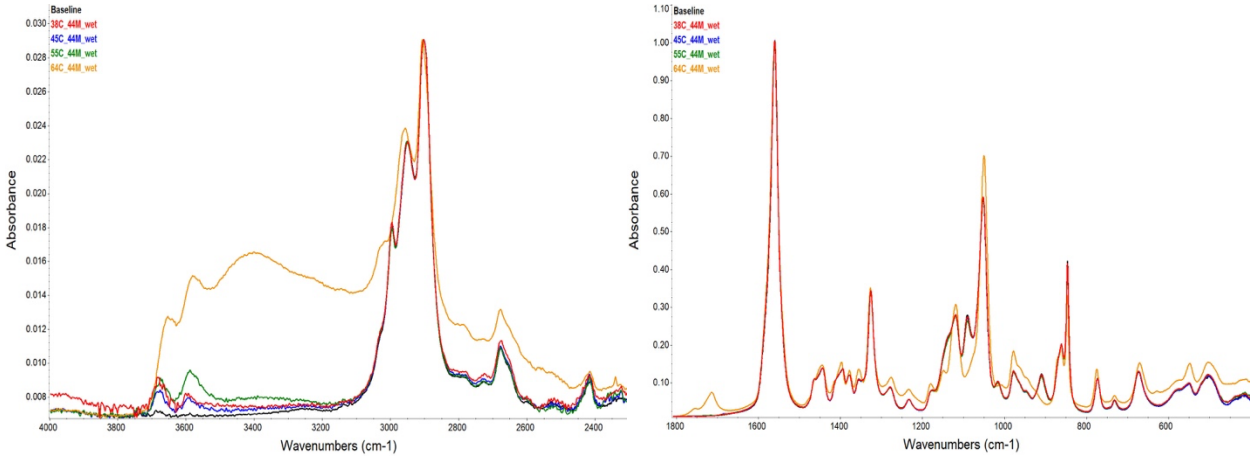

Figure 8. FTIR of the wet samples aged for 44 months at different temperatures. All spectra are normalized at highest peak respective to the HWN and LWN regions.

Table 3(a). Tentative assignment for the key peaks found in the FTIR spectra of BDNPA, BDNPF, NP, and fragments from NP degradation (from 4000–1380 cm^{-1}) [1)] [30, 31]. Key: u –stretching, u_s – symmetric stretching, u_{as} – asymmetric stretching, d – scissoring.

BDNPA	BDNPF	NP	Degraded NP	Tentative Assignment
		3678 vvw	3678 vvw, sh	Free water [24]
			3600-3580 vw	HNO_2 [23]
			3580 - 3560 vw to w 3550	$HNO_3 \bullet H_2O$ [23, 28] [32]
			3470 w +/- 30	Poly-OH 2(>C=O)
			3450 w +/- 20	H_2O in HNO_3 [28]
			3380 m	HNO_3 liquid [28]
3266 vvw	3266 vvw	3260 vvw	3260 vvw (wet)	$(H_2O)_6$ cluster [24]
3038 vw	3034 vw	3030 vw, sh	3030 vw to w, sh	$\nu_{as}(CH_3)$
3003 w	3001 vw	2997 w	2997 w, up	$\nu_{as}(CH_2)$
2975 w, sh	2976 w			$\nu_s(CH_3)$
	2961 w			$\nu_s(O\text{-}CH_2\text{-}O)$
			2960 v	$HNO_3 \bullet H_2O$ [28]
2949 v		2951 v	2951 v, up	$\nu(>CH\text{-}CH_3)$ (from BDNPA)
			2920 vw	NO_2 [23, 33]
2895 w	2910 w	2903 w	2903 w	$\nu_s(CH_2)$
2680 vw	2684 vw	2678 vvw	2678 vvw, up	$2[\nu_s NO_2] + \nu(OH)$ [28]
2650 vw	2664 & 2641 vvw	2654 vvw, sh		$2[\nu_s NO_2]$
			2690 w, 2600 w (wet)	$NO_3^- \bullet HNO_3$, $H_2O \bullet HNO_3$ [28]
			2560 vvw, 2510 sh	HNO_3 vapor [28]
		2325 vw		NO_2^+ [28]
			1760 - 1730 w	>C=O
			1640 & 1720 w	NO_2 and N_2O_5 (NO_2+NO_3) /HNO_3 [23, 34]
			1710-1714 m	HNO_3 (vapor) [28, 35]
			1675-1680 w	H_3O^+, HNO_3 [28, 35]
1560 vs	1555 vs	1560 vs	1562 vs	$\nu_{as}(NO_2)$
1465 w	1467 w	1464 w, sh	1464 w, sh down	$\delta(CH_2)$
1443 w, sh	1443 m	1444 w	1446 w, up	$\delta_{as}(CH_3)$
			1440 vw	δ_{as}, $_s(NO_2)$ from -ONO [34]
1411 w	1414 vw, sh	1410 w, sh	1410, w, sh up	$\nu(CO\text{-}CH_2)$
1395 w	1401 m	1395 w	1398 w (more F)	$\delta_s(CH_3)$
1384 w				$\nu(CO\text{-}CH_2) + \delta(CH_3)$ (from BDNPA)
			1384 sh, up	NO_3^-, N_2O_5 +H_2O [34]

[1)]: vvw – very very weak, vw – very weak; w – weak; m – moderate; s – strong; vs – very strong; sh – shoulder.

Table 3(b). Tentative peak assignment in BDNPA, BDNPF, NP, and fragments from NP degradation in their FTIR spectra (1380–450 cm^{-1})[1)]. Key: u –stretching, u_s – symmetric stretching, u_{as} – asymmetric stretching w – wigging, d – scissoring, ρ – rocking, def. – deformation.

BDNPA	BDNPF	NP	Degraded NP	Tentative Assignment
1374 w	1375 w	1379 w	1379 w, up	$\nu(CO\text{-}CH_2) + \delta(CH_2)$
			1366 m	HNO_3 (2.8 mole%) [28]
1359 w	1355 w	1356 w	1355 w, up	$\nu(CO\text{-}CH_2) + \delta(CH_2)$
			1340 w, up	NO_3^- [23], N_2O_5/HNO_3 [32]
1325 m	1331 m	1327 m	1326 m	$\nu_s(NO_2)$
			1263 m	HONO [23, 33, 35]
1279 w	1266 w	1278 w	1279 w, up	ν(CN), ν(-C-OH),
1238 w	1225 w	1233 vw	1233 w, sh	ν_{as}(-COC-)
			1220 w (dry), up	HNO_3 (vapor) [28]
	1180 w	1176 w	1178 w, up	ν_{as}(-COC-), ν(-C-OH)
	1151 vw			ν_{as}(-COC-) [$O(CH_2)O$] (from BDNPF)
1137 s		1137 m, sh	1137 m, sh, down	ν_{as}(-COC-) [$-CH_2OCH<$] (from BDNPA)
1115 m	1119 s	1120 m	1120 m, down	ν_s(-COC-)
1092 m		1091 m	1090 m to w, down more	ν_s(-COC-) [$-CH_2OCH<$] (from BDNPA)
1064 s	1060 s	1053 s	1053 s, down	ν_s(-COC-)
1015 m		1017 w	1017 w, up	ν_s(-COC-) [$-CH_2OCH<$] (from BDNPA)
976 w	977 m	978 m	978 m, up	ν(-CNO-), ν(-CCOOH),
948 w	945 w	948 w, sh	949 w, sh up	δ(N-O)
910 m		910 w	910 w, down more	δ_s (COC) [$-CH_2OCH<$] (from BDNPA)
865 s[2)]	878 s[2)]	862 m	862 m	$\nu(C\text{-}NO_2)$ + C=C-H
847 m[2)]	850 m[2)]	847 s	847 m, down	ν(C-N) + C=C-H
774 m	772 s	774 w	774 w, up	δ(O-N=O) [28]
733 w	729 w	732 w	732 vw	$\rho(CH_2)$
674 m	680 s	674 m	672 w, up	$CH_3\text{-}CH_2\text{-}NO_2$ nitroethane
			630 w, up	$\omega(H\text{-}NO_2)$
			602 sh, up	HNO_3 (vapor) [28]
557 m	556 w	550 w	555 w, up	-OH, def.(COH)
518 & 503 m	510 m	506 w	501 w, up	-OH, def. (COH)

[1)]: vvw – very very weak, vw – very weak; w – weak; m – moderate; s – strong; vs – very strong; sh – shoulder.
[2)]: These peaks were only labeled as $–CH_n$ bending in our previous paper [36].

4.2.2. Environment effect

Figure 9 shows a set of FTIR spectra obtained from air, N_2, and wet samples aged for 44 months in various environments, at 45°C (top row), 55°C (middle row) and 64°C (bottom row). The FTIR spectrum of the baseline NP is also included. At 45°C, for all three samples, the lack of spectral changes between 3000 and 700 cm^{-1}, compared to the spectrum of baseline NP, suggests that the backbone structure of these aged NP samples remains the same. Even though there are some changes in the region of 3000-

4000 cm^{-1}, they are mostly related to the states of water molecule arrangements (free vs. clustered) due to the variation of exposed environments. Overall, if there is some degradation, the structural changes are not detectable in their FTIR spectra after the samples aged at 45°C for 44 months regardless of aging environments.

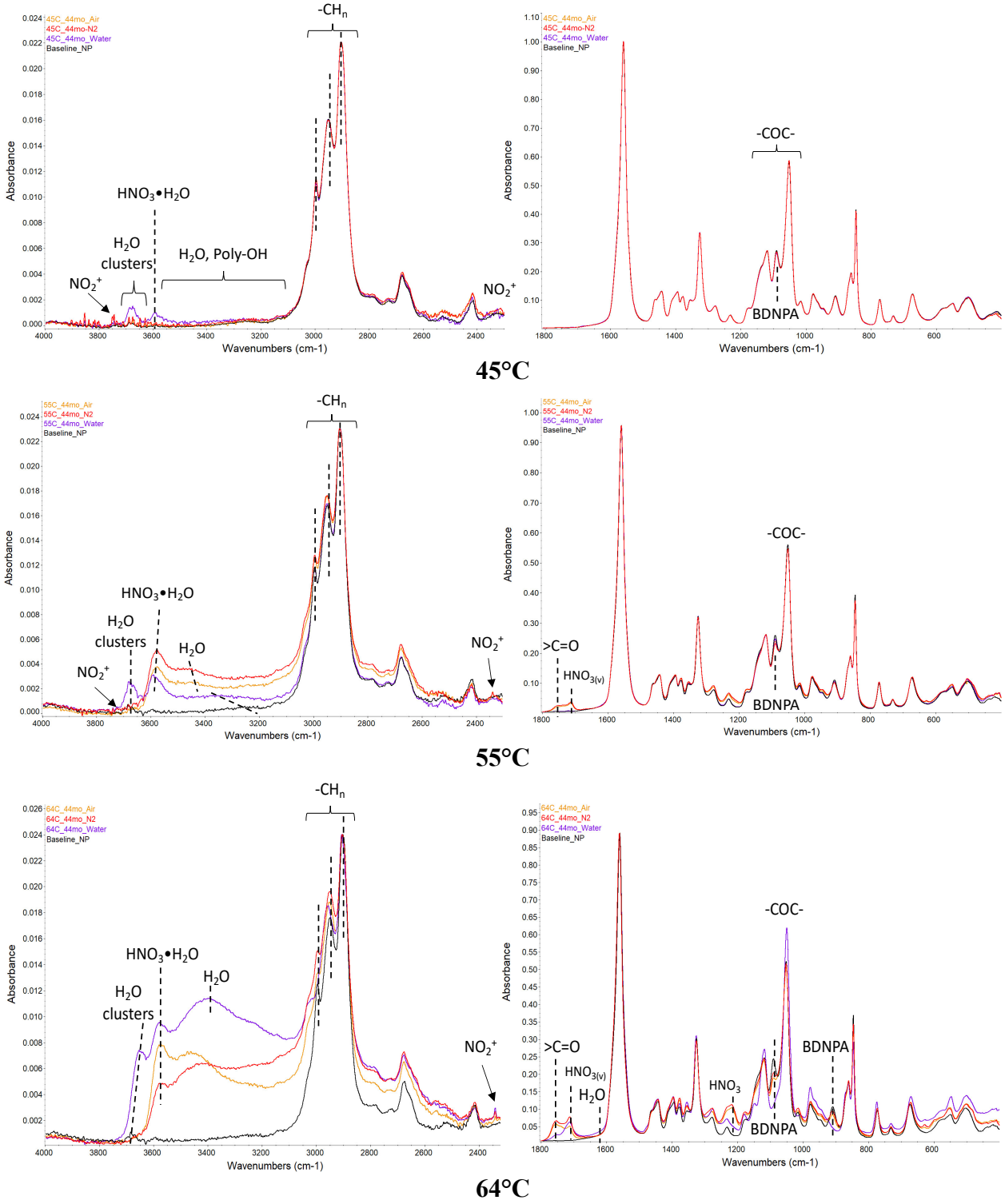

Figure 9. FTIR spectra of the samples aged inside the vials at various temperatures for 44 months.

At 55°C, noticeable changes are detected, as shown in Figure 9 (middle). For the wet sample, the intensity of the nitronium ion (NO_2^+) peak (~3740 cm^{-1}) decreases, the HNO_3 peak (~3585 cm^{-1}) increases compared to the result of the wet sample aged at 45°C. Considering the low water concentration (<3000 ppm) in the wet samples, we suspect that local HNO_3 concentration in some region is high even though its bulk concentration is small. Since the baseline NP is more than 51 years old, it actually contains a trace amount of HNO_3, and possible NO_2^+ species. When aged in direct contact with water, water concentration increases in the NP phase from ~760 ppm to up to 3000 ppm, which allows the equilibrium of $NO_2^+ NO_3^- + H_2O \Leftrightarrow 2HNO_3$ shifts forward. Accordingly, the intensity of the small water cluster at ~3680 cm^{-1} increases and ends up outgrowing the ~3350 cm^{-1} peak, suggesting that the number of the water molecules in the clusters is reduced, i.e., from 5 to 3. This observation can be explained in the following way. As the temperature increases from 45°C to 55°C, the HNO_3 concentration increases due to more aggressive degradation. Furthermore, more available water molecules dissociate HNO_3 into ionic form - H_3O^+ and NO_3^-, instead of forming $HNO_3 \bullet (H_2O)_n$ water clusters. As a result, the acidity increases, compared to the wet sample aged at 45°C. For the dry (air and N_2) samples, the spectral changes are different from those observed from the wet sample. There is no peak detected at 3680 cm^{-1}, but the intensity of the peaks between 3600 cm^{-1} and 3200 cm^{-1} is higher than that in the wet sample. Accordingly, a tiny peak at 2340 cm^{-1}, associated with NO_2^+, grows in the dry samples. The water peak between 3500 and 3200 cm^{-1} shifts from ~3350 cm^{-1} in the wet sample to ~3480 cm^{-1}. The peak of HNO_3 vapor (v) at 1710 cm^{-1} is only detected in the dry samples. The BDNPA peak at 1093 cm^{-1} also decreases more in the dry samples than in the wet sample. Additionally, two new peaks between 1800 and 1600 cm^{-1}, associated with >C=O group (~1760 cm^{-1}) and $HNO_{3(v)}$ molecules (~1710 cm^{-1}), respectively, are only detected in the dry samples as well. All these comparative results suggest that 1) the dry samples do not contain a large amount of water clusters, but do contain more H-bonded water molecules; 2) the concentration of $HNO_3 \bullet (H_2O)_n$ (peak at 3580 cm^{-1}) in the dry sample is higher than in the wet sample, which is also responsible for the higher intensity of the NO_2 peak at ~2680 cm^{-1} in the dry samples than in the wet sample; and 3) NP hydrolysis is more advanced in the dry samples than the wet sample when both of them are aged at 55°C for 44 months. These observations suggest that the excess amount of water in the wet sample dilutes the HNO_3 concentration so to reduce the acid-catalytic effect. Furthermore, some acidic molecules are removed from the NP phase into the aqueous phase.

At 64°C, spectral difference among three samples grows even larger than that found at 55°C and below, as shown in Figure 9 (bottom). Based on the FTIR spectral information provided by Marcus et. al. [28], the concentration of nitric acid was estimated to be between 25 wt% and 70 wt% in the wet samples, and maybe as high as 95 wt% and even exists in an anhydrate form in the dry samples. The spectral changes in the 3200–2800 cm^{-1} region are dramatic, compared to those found at lower temperatures: while the intensity of the C-H peaks grows noticeably in the dry samples, the CH_2 peak at 3000 cm^{-1} – a characteristic peak of BDNPA, completely disappears in the wet sample. Accordingly, the BDNPA peak at 1090 cm^{-1} completely disappears, suggesting that the -$COCH(CH_3)O$- functional group in BDNPA is destroyed through acetal hydrolysis in the wet sample. However, the -$COCH(CH_3)O$- group in BDNPA in the dry samples is still detected. All these observations suggest the less degree of hydrolysis occurring in the dry samples than that in the wet sample. On the contrary, the >C=O peak at

1760 cm^{-1} is more intense in the dry samples than in the wet samples, suggesting that the dry samples were oxidized more than the wet samples. All these spectral changes reveal that NP degrades differently under the dry and the wet environments. While BDNPA is preferably degraded through hydrolysis over oxidation under the wet condition, both BDNPA/F are oxidized to a greater degree in the dry condition than that in the wet condition when they are aged at 64°C for 44 months.

4.2.3. Headspace effect

Since the initial NP degradation involves volatiles formation (e.g., NO_x, H_2O, HNO_x, and N_2O), headspace composition will critically influence its cascading effect on the aging behavior of NP due to the suspected autocatalytic effect. To investigate this effect, we compare FTIR spectra, as shown in Figure 10, collected from two sets of samples aged at different containers: one set was aged in the sealed container and the other was aged in the leaked container. However, both sets of samples had been aged at 64°C for 44 months under either the dry (top row) or the wet environment (bottom row).

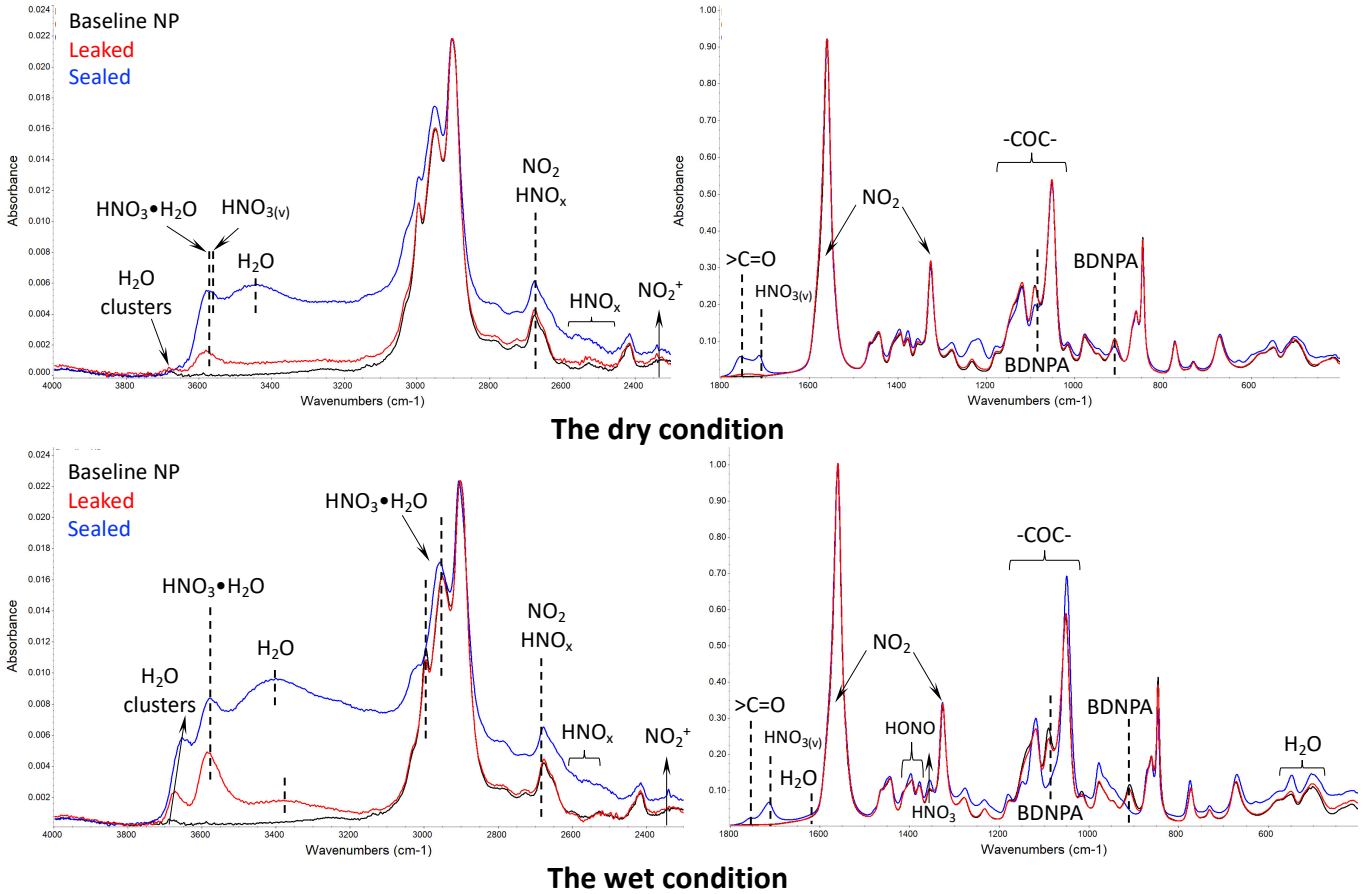

Figure 10. FTIR spectra of the leaked samples (red lines) and the sealed samples (blue lines) under the dry condition (top) and under the wet condition (bottom) at 64°C for 44 months.

Regardless of the aging environments, larger spectral changes are observed for the sealed samples compared with leaked samples. Aging at 64°C for 44 months, the intensities of the HNO_3 (at ~3580 cm^{-1}) and water/acid cluster (at 3400–3200 cm^{-1}) peaks in the leaked samples grow noticeably, compared to those in the baseline sample. However, no significant changes are seen between 3000 cm^{-1} and 450 cm^{-}

[1] except for a small decrease in the intensity of BDNPA peaks at 1093 and 910 cm^{-1} under the wet condition, suggesting that some hydrolysis occurred in the leaked sample aged under the wet condition, but not noticeable in the leaked sample aged under the dry condition. Conversely, in the sealed samples, the intensities of the HNO_3 (at ~3580 cm^{-1}) and water/acid (at 3400–3200 cm^{-1}) peaks grow significantly in the HWN region. Accordingly, the intensity of the >C=O peak (at ~1760 cm^{-1}) and $HNO_{3(v)}$ (at 1710 cm^{-1}) peaks grows noticeably in the LWN region. All these large changes in the FTIR spectra of the sealed samples suggest that the accumulated volatiles can not only serve as reactants, but also as catalysts to accelerate oxidative and hydrolysis processes in the sealed samples. Elevated temperatures will enhance their auto-catalytic effects. As a result, the backbone structure of NP is severely changed through oxidation under the dry condition and through hydrolysis under the wet condition. Due to the reactivity and auto-catalytic effects of the accumulated products, NP degradation will be more advanced in a closed system that in a leaked system. This comparison indirectly demonstrates the effect of the headspace composition on the aging behavior of NP.

5. Conclusions

In the past several years, we have conducted a systematical aging experiment and attempted to understand how NP degradation starts and progresses under various conditions. Together with our previous publications and the work presented here, we have a much better understanding of the reaction mechanisms involved in the NP aging under moderate temperatures (<70°C). The major fundings and achievements of these studies are:

1) DFT calculations are performed using the complete molecules of BDNPA and BDNPF. The calculated activation energy and Helmholtz free energy for the HONO elimination and HONO re-addition are almost the same as those found in the previous study when the "half of a BDNPA" molecule was used (in earlier work). One end of the complete molecule has negligible influence on the other end. For the HONO re-addition, the HO-NO re-addition to form nitroso alcohols isomers is more energetically favorable than the H-ONO re-addition to form nitrite isomers.
2) DFT calculations are further used to compare the activation energy and Helmholtz free energy of four reactions: HONO elimination, NO_2 homolysis, reaction with water reaction, and reaction with a proton. The results suggest that under a pH neutral environment, HONO elimination is the most energetic favorable reaction. NO_2 homolysis requires more than two times higher activation energy to proceed. *Water does not react with BDNPA and BDNPF under the moderate temperatures.* However, in the presence of proton, NP hydrolysis can occur. As the acidity increases, the activation energy of NP hydrolysis changes from positive to negative, which explains why there is an acidity threshold to trigger the NP hydrolysis.
3) NP degradation exhibits two stages: early and later.
    a. In the early stage, HONO elimination is a key product through NP oxidation degradation. Due to its instability, HONO can decompose into water, NO and NO_2. These are reactive molecules that can further degrade NP via different reactions pathways, depending on the surrounding environment and temperatures. Overall degradation progresses very slowly (less than 1-2 wt%) in the early stage due to the protection PBNA and its derivatives [37]. The bulk properties of NP are well preserved.

b. In the later stage, as the efficiency of the antioxidants decreases, the concentration of HNO_3 increases. When HNO_3 concentration is higher than 1.35 mM, NP degradation rapidly progresses into the secondary stage in which it is predominately degraded through acid-catalyzed hydrolysis [20]. Elevated temperatures accelerate this degradation process, which can greatly change the bulk properties of NP.

4) In our early work, we have suggested that BDNPA can preferentially degrade over BDNPF. However, the DFT calculations in the current study suggests that the activation energy and Helmholtz free energy for both BDNPA and BDNPF are very compatible via the HONO elimination reaction. On the other hand, the DFT simulations predict that BDNPA is more prone to hydrolysis than BDNPF under the acidic condition. These results explain why the BDNPA/F ratio is often observed unchanged when NP degrades predominantly through HONO elimination. However, once NP largely degrades, the BDNPA/F ratio largely decreases. Depending on the type of NP degradation, the BDNPA/F ratio might not properly reflect the property changes in aged NP.
5) Since compounds generated from HONO decomposition are volatile, the surrounding environment significantly alters the reaction pathways followed. At low temperatures (below 55°C), an excess of water slows down NP degradation through the chemical equilibrium of $2HONO \leftrightarrow H_2O + NO + NO_2$. Over dry condition under extensive evacuation the NP phase can trigger more HONO decomposition and hence accelerates the PBNA consumption and NP degradation.
6) Since headspace composition significantly impacts the aging behavior of NP, in future aging experiment design, the headspace volume of an aging container must be rigorously controlled as tight as possible to mimic the aging conditions when NP is involved in these applications.

Finally, by taking advantage of the knowledge gained from the previous studies, and the insights obtained from different characterization methods, the obtained wealth of information not only verifies the previously proposed mechanisms, but also identifies new reaction mechanism(s) occurring in the real-world application conditions. The ultimate goal of future LC/QTOF and IC studies is to build an extended library of degraded products and fragments, which could be used to search and identify the products found inside the stockpile. The compared results would help us predict the degree of degradation of the PBX 9501 inside the stockpile and thus help to predict the lifetime performance of PBX 9501 materials under various application conditions.

ACKNOWLEDGMENTS

We thank Justine Yang for aging sample preparation and some KF and FTIR analyses. We thank Kitmin Chen, Alex Edgar, Joel Kress, Cameron Moore, Paul Peterson, Robert Gilbertson, Phil Leonard, Troy Holland, and Brennan Billow for fruitful discussion of NP degradation topic in general. This research *used resources provided* by Los Alamos National Laboratory Aging and Lifetimes Program and *by the Los Alamos National Laboratory Institutional Computing Program*. Los Alamos National Laboratory is

operated by Triad National Security, LLC, for the National Nuclear Security Administration of the U.S. Department of Energy (Contract No.89233218CNA000001).

References:

[1] S.-M. Shen, Y.-S. Chiu, S.-I. Chen, Thermal characteristics of poly-BAMO and poly-BAMO/BDNPA/BDNPF blends, Thermochimica Acta 213 (1993) 151-164.
[2] A. Provatas, Energetic Polymers and Plasticisers for Explosive Formulations - A Review of Recent Advances, Aeronautical and Maritime Research Laboratory, Melbourne Victoria 3001 Australia, 2000, p. 51.
[3] D. Wrobleski, D. Langlois, E. Orler, D. Dattelbaum, J. Small, Application of ^{15}N labeling for oxidative degradation study of a plasticized poly(ester urethane), Polymer Preprints 45(1) (2004) 789-790.
[4] D. Yang, A.S. Edgar, J.A. Torres, Jillian C. O'Neel, A Progress Report for a 44-month Aging Study on Nitroplasticizer (NP) Stability – Summary of KF and TGA Results, Los Alamos National Laboratory, LA-UR-23-26032, Los Alamos, New Mexico, 2023.
[5] D. Yang, J.A. Torres, K. Cluff, A.S. Edgar, Stability of Naturally Aged Nitroplasticizer, Los Alamos National Laboratory Report: LA-UR-18-23141, Los Alamos, New Mexico, 87545, 2018, pp. 1-17.
[6] D. Yang, A.S. Edgar, J.A. Torres, J.C. Adams, J.D. Kress, Thermal Stability of a Eutectic mixture of Bis(2,2-dinitropropyl) Acetal and Formal: Part C. Kinetic Compensation Effect, Propellants, Explosive, Pyrotechnics 46 (2021) 134-149.
[7] D. Yang, D.Z. Zhang, Role of water in degradation of nitroplasticizer, Polymer Degradation and Stability 170 (2019) 109020.
[8] F. Neese, The ORCA program system, WIREs Comput Molecular Science 2 (2012) 73-78.
[9] F. Neese, Software update: The ORCA program system - Version 5.0, WIREs Comput Mol Sci 12(5) (2022) 1-15.
[10] S. Grimme, J. Antony, S. Ehrlich, H. Krieg, A consistent and accurate ab initio parametrization of density functional dispersion correction (DFT-D) for the 94 elements H-Pu, The Journal of Chemical Physics 132 (2010) 154104.
[11] V. Barone, M. Cossi, Quantum Calculation of Molecular Energies and Energy Gradients in Solution by a Conductor Solvent Model, J. Phys. Chem. A 102 (1998) 1995-2001.
[12] D. Yang, M.H. Yang, A.S. Edgar, Characterization of Various Materials Using Refractometry, Los Alamos National Laboratory, LA-UR-19-28628, Los Alamos, New Mexico, 87545, 2018, pp. 1-18.
[13] A.L.H. Duque, W.L. Perry, C.M. Anderson-Cook, Complex Microwave Permittivity of Secondary High Explosives, Propellants Explos. Pyrotech. 39 (2014) 275-283.
[14] J. Zheng, Y. Zhao, D. G. Truhlar, The DBH24/08 Database and Its Use to Assess Electronic Structure Model Chemistries for Chemical Reaction Barrier Heights, J. Chem. Theory Comput. 5(4) (2009) 808-821.
[15] N.Mardirossian, M. Head-Gordon, Thirty Years of Density Functional Theory in Computational Chemistry: an Overview and Extensive Assessment of 200 Density Functionals, Molecular Physics 115(19) (2015) 2315-2372.
[16] D.K. Pauler, N.J. Henson, J.D. Kress, A mechanism for the decomposition of dinitropropyl compounds, Physical Chemistry Chemical Physics 9 (2007) 5121-5126.
[17] C.F. Melius, M.C. Piqueras, Initial Reaction Steps in the Condensed-Phase Decomposition of Propellants, Proceedings of the Combustion Institute, 2002, pp. 2863-2871.

[18] D. Yang, R. Pacheco, S. Edwards, K. Henderson, R. Wu, A. Labouriau, P. Stark, Thermal Stability of a Eutectic Mixture of Bis(2,2-dinitropropyl) acetal and formal: Part A. Degradation Mechanisms in Air and under Nitrogen Atmosphere, Polymer Degradation and Stability 129 (2016) 380-398.
[19] D. Yang, R. Pacheco, S. Edwards, J. Torres, K. Henderson, M. Sykora, P. Stark, S. Larson, Thermal Stability of a Eutectic Mixture of Bis(2,2-dinitropropyl) acetal and formal: Part B. Degradation Mechanisms under Water and High Humidity Environments, Polymer Degradation and Stability 130 (2016) 338-347.
[20] K. Chen, A.S. Edgar, Z. Li, O.C. Marina, D. Yang, Roles of HNOx and Carboxylic Acids in Thermal Stability of Nitroplasticizers, ACS Omega 8(16) (2023) 14730-14741.
[21] K.D. Morris, J. Cook, C. Harrison, X. Rodriguez, Evaluation of Nitroplasticizer Reserves, Level 2 Milestone ID 7134, Consolidated Nuclear Security, IIc. Pantex Plant PXRPT 20-10, Amarillo, TX, 2020, p. 157.
[22] K.D. Morris, Aged Nitroplasticizer Evaluation, PXRPT 22-01, CNS, IIC. Pantex Pant, 2022, p. 88.
[23] A.V. Pipa, J.r. Röpcke, Analysis of the Mid-Infrared Spectrum of the Exhaust Gas From an Atmospheric Pressure Plasma Jet (APPJ) Working With an Argon–Air Mixture, IEEE Transactions on Plasma Science 37(6) (2009) 1000-1003.
[24] M. Miyazaki, A. Fujii, T. Ebata, N. Mikami, Infrared Spectroscopy of Size-Selected Benzene-Water Cluster Cations [C6H6-(H2O)n]+(n = 1-23): Hydrogen Bond Network Evolution and Microscopic Hydrophobicity, J. Phys. Chem. A 108(48) (2004) 10656-10660.
[25] M.R. Salazar, S.L. Thompson, K.E. Laintz, T.O. Meyer, R.T. Pack, Degradation of a Poly(ester urethane) Elastomer. IV. Sorption and Diffusion of Water in PBX 9501 and Its Components, Journal of Applied Polymer Science 105(3) (2007) 1063-1076.
[26] J.B. Paul, C.P. Collier, R.J. Saykally, J.J. Scherer, A. O'Keefe, Direct Measurement of Water Cluster Concentrations by Infrared Cavity Ringdown Laser Absorption Spectroscopy, J. Phys. Chem. A 101 (1997) 4.
[27] A.S. Edgar, J.H. Yang, M.E. Chavez, M.H. Yang, D. Yang, Physical Characterization of bis(2,2-dinitropropyl) acetal and bis(2,2-dinitropropyl) formal, Journal of Energetic Materials (2020) 21.
[28] R.A. Marcus, J.M. Fresco, Infrared Absorption Spectra of Nitirc Acid and Its Solution, The Journal of Chemical Physics 27(2) (1957) 5.
[29] M.C. Celina, E. Linde, E. Martinez, Carbonyl Identification and Quantification Uncertainties for Oxidative Polymer Degradation, Polymer Degradation and Stability 188 (2021) 21.
[30] K. Nakanishi, Infrared Absorption Spectroscopy - Practical, Nankodo Company Limited, San Francisco, 1962.
[31] G. Socrates, Infrared and Raman Characteristic Group Frequencies Third ed., John Wiley & Sons, LTD, New York, 2001.
[32] C.A. Cantrell, J.A. Davidson, A.H. McDaniel, R.E. Shetter, J.G. Calvert, Infrared Absoption Cross Section for N_2O_5, Chemical Physics Letters 148(4) (1988) 358-363.
[33] H. Akimoto, H. Takagi, F. Sakamaki, Photoenhancement of the Nitrous Acid Formation in the Surface Reaction of Nitrogen Dioxide and Water Vapor: Extra Radical Source in Smog Chamber Experiments, International Journal of Chemical Kinetics 19 (1987) 593-551.
[34] W. Junkermann, T. Ibusuki, FTIR Spectroscopic Measurements of Surface Bond Products of Nitrogen Oxides on Aerosol Surfaces - Implications for Heterogeneous HNO_2 Production, Atmospheric Environment 26A(17) (1992) 5.
[35] M. Mochida, B.J. Finlayson-Pitts, FTIR Studies of the Reaction of Gaseous NO with HNO3 on Porous Glass: Implications for Conversion of HNO3 to Photochemically Active NOx in the Atmosphere, The Journal of Physical Chemistry A 104(43) (2000) 7.

[36] D. Yang, K.M. Hubbard, K.C. Henderson, A. Labouriau, Thermal and Chemical Stabilization of Ethylene/Vinyl Acetate/Vinyl Alcohol (EVA-OH) Terpolymers Under Nitroplasticizer Environments, J. of Applied polymer Science 132(17) (2015) 41450 (1-17).
[37] K. Chen, A.S. Edgar, J. Jung, J.D. Kress, C.H. Wong, D. Yang, Liquid Chromatography Quadrupole Time-of-Flight Mass Spectrometry Analysis of Eutectic Bis(2,2-dinitropropyl) Acetal/Formal Degradation Profile: Non-targeted Identification of Antioxidant Derivatives, ACS Omega 7(39) (2022) 35316-35325.